Heliyon 10 (2024) e30302

Contents lists available at ScienceDirect

Heliyon

journal homepage: www.cell.com/heliyon

Research article

Revealing the inherent running mechanism of quadruped mammals based on a novel bionic stiffness model

Yi Zheng [a,b,*], Sixian Rao [a], Jiapeng Gao [a]

[a] School of Mechanical Engineering, Anhui University of Technology, Ma'anshan, 243032, China
[b] Anhui Province Key Laboratory of Special Heavy Load Robot, Ma'anshan, 243032, China

ARTICLE INFO

Keywords:
Bionics
Nonlinear stiffness
QIPJCS model
Numerical simulation
Gallop
Running mechanism

ABSTRACT

In this paper, the limb of a goat is chosen as the research object, and according to mammalian anatomy, a bionic model called the quasi inverted pendulum with "J" curve spring (QIPJCS) model with nonlinear stiffness is built, and the equations of motion are derived. Based on these equations, the advantages of the QIPJCS model are illustrated from the aspect of the stable motion region by the SFA (step-to-fall analysis) numerical simulation method. These results are compared with the traditional SLIP model. Furthermore, the ARM (Apex-Return-Map) of this model is built, and the fixed points are analyzed. Finally, according to the locomotion law of goats running with gallop gaits and the analysis of the dead-point support effect, the dynamic motion mechanism of goat limbs is elucidated, and the equivalent mechanism model is built. Based on the mechanism, the dynamic mechanical analysis indicates that the joint driving torque can be minimized to conserve energy by optimizing the landing angle. The running mechanism research of quadruped mammals, which is based on the novel bionic stiffness model, provides theoretical support for the design of high-performance mechanical legs and the motion control of bionic robots.

1. Introduction

A great variety of 1.2–1.5 million species exist in the natural world. In the long term, these animals have made great contributions to the study of the natural universal truth for humans. Among these animals, mammals have attracted extensive attention from scholars in various disciplines due to their greater similarity with humans in physiological structure. Moreover, in the field of robotics, legged mammals provide rich templates for the development of legged robots. Changes in the physiological structure and motion characteristics of animals after continuous evolution are related to their living environments. The locomotion of most terrestrial mammals is dependent on limbs, which mainly include quadrupedal and bipedal movement. On the basis of the different living environments, species with larger limbs, such as ruminants, generally achieve faster running speeds. Correspondingly, species with smaller limbs, such as rodents, achieve more flexible motion ability in narrow spaces. Therefore, different animals exhibit different movement patterns according to their own structural characteristics and their living environments.

The coordinated function of the animal skeletal system and muscle system is conducive to the movement processes of animals. Moreover, different systems play different roles: the skeletal system, which consists of different types of bones and their articulations, confers basic functions such as organ protection and body support; the muscle system mainly serves a driving and controlling role during movement to accomplish a series of gaits. For different quadruped mammals, the modes of motion, such as walking and

* Corresponding author. School of Mechanical Engineering, Anhui University of Technology, No. 1530 Maxiang Road,Ma'anshan, 243032, China.
E-mail address: yiz@ahut.edu.cn (Y. Zheng).

https://doi.org/10.1016/j.heliyon.2024.e30302
Received 20 February 2024; Received in revised form 23 April 2024; Accepted 23 April 2024
Available online 27 April 2024

running, are similar. In addition, quadruped animals can realize locomotion by jumping, and the energy efficiency of jumping is higher than that of other gaits [1].

Currently, great progress has been made in the research field of legged robots through the tireless efforts of worldwide scholars. Various biomimetic legged robots have been developed and employed in various fields, such as emergency rescue, military transportation and entertainment services [2–5]. Even so, the locomotion performance of animals is still far superior to the locomotion performance of the corresponding biomimetic legged robots: for example, the high-speed running of the cheetah [6], the stable jumping of the kangaroo [7], the flexible climbing of the goat [8], etc., cannot be perfectly realized by corresponding biomimetic robots at the present stage. For instance, the first generation of Cheetah quadruped robots [9–14], which was developed by MIT, achieves a maximum running speed of 6 m/s; however, the maximum running speed of the bionic template, acinonyx jubatus, is 29 m/s [15]. Moreover, these remarkable locomotion abilities of animals are closely related to the stiffness characteristics of their limbs [16]. Hence, in the research of the mechanical leg stiffness design of legged robots, the stiffness characteristics of animal limbs provide important reference templates for design. In this paper, according to the physiological structure and locomotion characteristics of large quadruped mammals, the bionics mechanism is analyzed, and the corresponding bionic mapping model is built. Based on this model, the locomotion performance is studied through simulation analysis. This model can be employed as a template to guide the design of biomimetic mechanical legs for legged robots. Finally, the internal running mechanism of animal dynamic motion is analyzed by combining the bionic model with natural gait.

This paper is structured as follows. The QIPJCS model based on biological leg stiffness is introduced in Section 2: this section includes the locomotion characteristic analysis, which is based on the quadruped mammal anatomy, the construction of the bionic mapping model and the derivation of the dynamic equation of this model. In Section 3, we compare the locomotion performance of the QIPJCS model with that of the classical SLIP model by using numerical simulation analysis in the ideal and completely passive locomotion states. The stable motion region analysis is simulated by utilizing the SFA method. Moreover, the ARM of the QIPJCS model is built, and the fixed point, which can also influence the dynamic performance of the model, is analyzed. In Section 4, the equivalent mechanism sketch with sequential changes in goat dynamic motion is constructed by combination with the dead-point support effect of animal limbs in the process of galloping. In addition, the equation of joint torque optimization with landing angle adjustment is completed based on the mechanics performance analysis. Section 5 concludes this paper.

2. Equivalent QIPJCS model of a goat limb

Currently, relevant scholars have carried out related research on the mechanism of model stiffness acting on locomotion performance. The spring-loaded inverted pendulum (SLIP) model [17] and two-segment leg (TSL) model [18] are mainly employed in this research. Meanwhile, many submodels are derived from the application of these two models, such as the D-SLIP model [19], TSLIP model [20], and three-segment leg model [21]. However, considering that the flexible structure in the SLIP model is a spring with linear stiffness and is a linear stiffness joint in the TSL model, the biological limb stiffness is determined by a complex tension system composed of muscles, tendons, ligaments and bones and exhibits an obvious nonlinearity. Therefore, we will draw on the classical model describing the locomotion and the simplification of the complex tension system as a reference. Subsequently, we start with the stiffness of the flexible biological limb system and then combine it with a rigid system such as the skeleton. Finally, the biomimetic stiffness foundation model, which is more in line with the locomotion characteristics of biological limbs, is built.

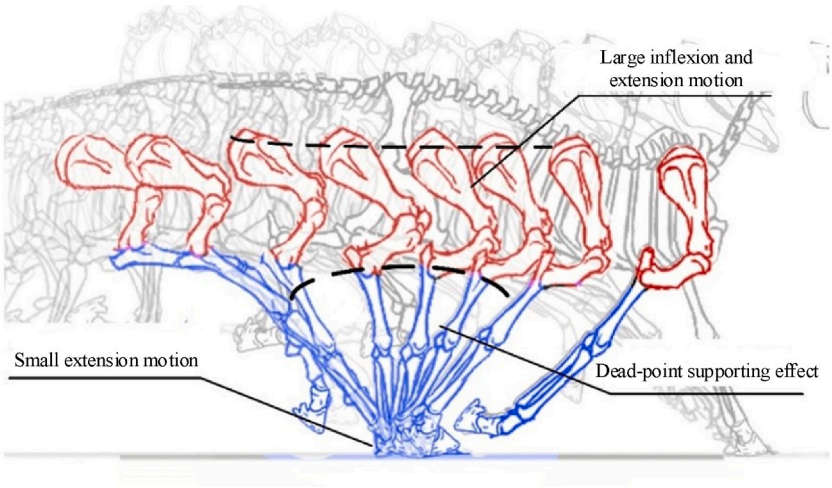

Fig. 1. The skeletal structure changes of goat forelimb in the foot-ground contact process.

2.1. QIPJCS modeling

Among the large quadruped mammals, most genera of ruminants possess good mobility (such as Cervidae) or high load capacity (such as Bovidae). Moreover, goats are quadruped mammals that live in the mountains [22]; not only does this species possess the ability for fast locomotion in flat areas, but goats can also flexibly climb in rugged areas. During the climbing process, the limbs are stressed by a greater support force from the ground. Hence, considering both the mobility and load capacity, goats are an ideal study subject for this research.

First, we can learn about the basic composition of goat limb bones from the goat anatomy [23]. This skeletal structure can be combined with the limb pose in the foot-ground contact process when the goat moves on the horizontal plane; then, the corresponding locomotion model of the goat skeletal system is built. Moreover, during the locomotion process, the key frame is extracted. Finally, the change law of the forelimb skeletal structure of large quadruped mammals such as goats in the foot-ground contact process can be obtained as shown in Fig. 1.

The skeletal structure morphology changes of the goat forelimb in the foot-ground contact process analysis are presented as follows. The foot-ground contact process of the forelimb can be divided into two parts: the touch-support process and the support-pedal process. The dividing line between these two processes is the plumb line, which passes through the foothold. The support state of a single limb in the locomotion process is similar to the dead-point support effect of the static support process [24]. For the limb mechanics analysis of large quadruped mammals with static standing, the scholars of Beihang University present the theory of the dead-point support effect, which reveals that the best support line or the best support posture under the dead-point support effect is the most comfortable state when the animal stands still. When the limb is in the state of dead-point support, the energy consumption by the musculature is minimal. Meanwhile, the sum of joint torques in joints is also the minimum. In this case, the burden upon the muscles can be reduced, which is beneficial for improving the load capacity of animals.

In general, before the animal foot touches the ground, the elbow joint and wrist joint have already rotated and established the radius and metacarpals in a straight line as far as possible. This state is similar to the morphology of the elbow joint and wrist joint under a static dead-point support state. Moreover, this state remains mostly unchanged during the entire foot-ground contact process. A small extension motion exists in the metacarpophalangeal joint during the touch-support process. When the metacarpophalangeal joint reaches the limit, this joint can cooperate with the elbow joint and wrist joint to convert the torque of the joint into the structural movement of the skeleton. During the touch-support process, the shoulder joint exhibits a flexion motion in addition to the swinging limb motion to realize the pose of the support state and minimize the shoulder joint torque. However, during the support-pedal process, the shoulder joint and the metacarpophalangeal joint exhibit an extension motion and a flexion motion, respectively. These motions can realize the swing of a single limb and increase the reactive force from the ground.

Therefore, during the foot-ground contact process, the elbow joint, wrist joint and metacarpophalangeal joint can maintain the state of dead-point support most of the time. As a consequence, the torque of the joint and energy consumption in locomotion can be reduced. In contrast, the swing amplitude of the shoulder joint is relatively large, and muscles, tendons, etc., in this joint serve the main roles in buffering and energy storage.

According to the analysis of animal physiological structure and the locomotion law mentioned above, the angle change of each joint below the elbow joint is small during the foot-ground contact process, and a dead-point support effect exists in this part of the limb. This can be explained by the rigid model of the inverted pendulum. Furthermore, flexible structures such as muscles, tendons, etc., exist in animal limbs, and these parts act as a means of buffering and storing energy in the process of animal locomotion. This can be

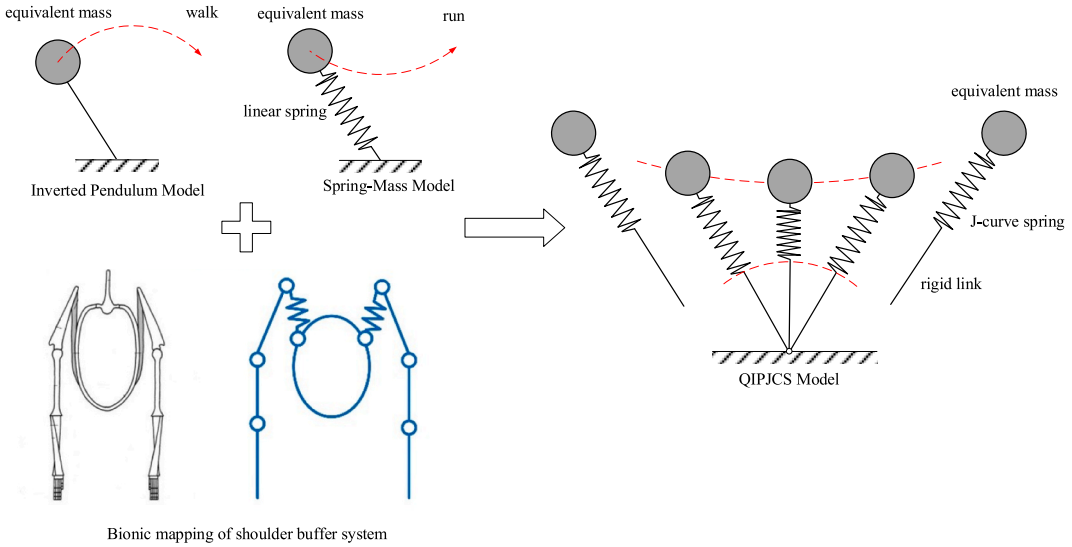

Fig. 2. Construction of the QIPJCS model.

explained by the flexible spring-mass model. Moreover, because the angle change of the shoulder joint is relatively large during the locomotion process, the muscles, tendons, etc., of the shoulder joint play leading roles in buffering and energy storage. Hence, a flexible structure that is similar to the spring exists between the body and limbs. Hence, we can draw on the experiences of animal walking with an inverted pendulum model and running with a spring-mass model [25] and then combine them with the flexible structure in the shoulder. We can build a motion model that is similar to the SLIP model, as shown in Fig. 2.

Similar to the SLIP model, the whole mass can be equivalent to a mass point at the top of the model. However, the multistage limb structure of animals in this model is not simply equivalent to a linear compression spring such as the SLIP model. Here, the multistage limb structure is equivalent to a structure that is composed of a nonlinear compression spring and a massless rigid link. We define this model as the QIPJCS (Quasi Inverted Pendulum with "J" Curve Spring) model.

For the nonlinear compression spring in the QIPJCS model, first, according to the extensive study of the characteristics of muscle stiffness and tendon stiffness of animal limbs from related scholars in the field of biology, such as the research of Couppe et al. on the human patellar tendon [26] and the research of Lichtwark et al. on horse pennate muscle [27], we draw the conclusion that most stiffness characteristics of soft tissues, such as muscles and tendons, can be described by a curve shaped like a "J". On this basis, Jutte et al. designed a nonlinear spring corresponding to this "J" curve stiffness [28]. As shown in Table 1, the five feature points describing the "J" curve spring are given. The elastic element of the QIPJCS model proposed above utilizes this nonlinear spring with "J" curve stiffness.

Based on this method, we can employ the five feature points of Table 1 to construct the $F-\Delta l^J$ equation with the characteristics of the "J" curve. Combined with curvilinear interpolation, this equation can be defined as follows:

$$F\left(\Delta l^J\right)=a_0+a_1\Delta l^J+a_2\left(\Delta l^J\right)^2+a_3\left(\Delta l^J\right)^3+a_4\left(\Delta l^J\right)^4, \tag{1}$$

Then, based on Equation (1) and Table 1, an equation set with five unknown coefficients is built. By solving this equation set, the $F-\Delta l^J$ equation can be further expressed as:

$$F\left(\Delta l^J\right)=\frac{4F_{\max}}{25l_{\max}}\Delta l^J-\frac{11F_{\max}}{25(l_{\max})^2}\left(\Delta l^J\right)^2+\frac{48F_{\max}}{25(l_{\max})^3}\left(\Delta l^J\right)^3-\frac{16F_{\max}}{25(l_{\max})^4}\left(\Delta l^J\right)^4, \tag{2}$$

where $l_{\max}$ is the maximum stretch length of the "J" curve stiffness spring and $F_{\max}$ is the corresponding force of $l_{\max}$.

Obviously, once the maximum stretch length $l_{\max}$ and the corresponding force $F_{\max}$ are determined, the stiffness characteristic of the "J" curve spring can also be determined.

According to the literature [29], in general, 10 % compression of the initial limb length is a typical value in the case of animal running. Hence, the force F in limbs can be normalized:

$$F_{\text{norm}}=\frac{F}{F_{10\%}}, \tag{3}$$

where $F_{10\%}$ is the force of the spring at 10 % compression.

A relevant biological study indicated that the maximum compression of animal limb muscle rarely exceeds 30 % of its initial length, even in high-speed running [25]. Hence, during the motion process, the maximum spring compression of the QIPJCS model can be set as 30 % of the rest spring length. Then, the variation in the spring should be normalized as well:

$$l^J_{\text{norm}}=\frac{\Delta l^J}{l^J_0}\times 100\%, \tag{4}$$

where l^J_0 is the rest length of the spring.

Based on Equations (2)–(4), the normalized force-length curves of the classical SLIP model and QIPJCS model are compared, as shown in Fig. 3.

2.2. The dynamics of the QIPJCS model

First, two hypotheses are proposed.

1. No relative movement exists between the foot and the ground (no slip occurs) during the whole foot-ground contact process. The kinematic constraint can be considered an ideal fixed hinge.
2. The collision is completely elastic at the moment of the foot touching the ground, and no damping exists in this spring (there is no energy loss). System energy is conserved in periodic locomotion.

Table 1
Five characteristic points of "J" curve spring.

Δl^J	0 %	25 %	50 %	75 %	100 %
F	0 %	4 %	17 %	48 %	100 %

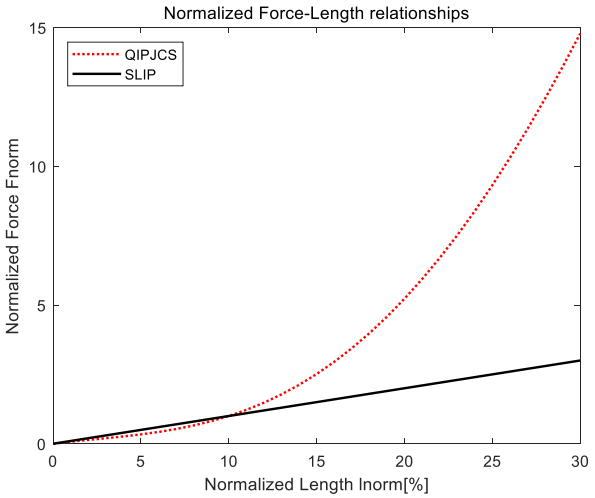

Fig. 3. The normalized force–length curves of the SLIP model and QIPJCS model.

As in the classical SLIP model, the locomotion process can be divided into two parts: flight phase and stance phase. The dynamic equation of the QIPJCS model in the flight phase is the same as that of the SLIP model:

$$\begin{cases} \ddot{x} = 0 \\ \ddot{y} = -g \end{cases}, \tag{5}$$

Then, the mathematical expression with the closed form is:

$$\begin{cases} x(t) = x(0) + \dot{x}(0)t \\ y(t) = y(0) + \dot{y}(0)t - \frac{1}{2}gt^2 \end{cases}, \tag{6}$$

In the stance phase, as shown in Fig. 4, the Lagrange function can be represented as follows:

$$L = \frac{1}{2}m\left(\dot{s}^2 + s^2\dot{\theta}^2\right) - mgs\cos\theta - V_{\text{spr}}, \tag{7}$$

$$L = \frac{1}{2}m\left(\dot{l}^{J2} + \left(l^{J2} + j^2 + 2l^J j\right)\dot{\theta}^2\right) - mgl^J\cos\theta - mgj\cos\theta - V_{\text{spr}}, \tag{8}$$

where m is the mass, s is the length of the rigid link and spring, θ is the angle between the rigid link and the normal of horizontal ground, V_{spr} is the elastic potential energy of the spring, l^J is the length of the spring, and j is the length of the rigid link.

The dynamic equation of the QIPJCS model in the stance phase can be represented as follows:

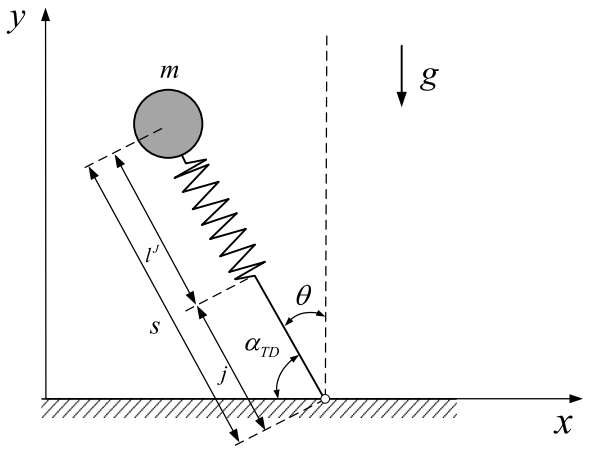

Fig. 4. The stance phase of the QIPJCS model.

$$\begin{cases} m\ddot{l}^{J} - m\left(l^{J}+j\right)\dot{\theta}^{2} + mg\cos\theta + f\left(\Delta l^{J}\right) = 0 \\ \dfrac{d}{dt}\left(m\left(l^{J2}+j^{2}+2l^{J}j\right)\dot{\theta}\right) - mg\left(l^{J}+j\right)\sin\theta = 0 \end{cases} \tag{9}$$

Substituting Equation (2) into the first equation of Equation (9):

$$m\ddot{l}^{J} + mgcos\theta - m\left(l^{J}+j\right)\dot{\theta}^{2} + \left(\frac{4F_{\max}}{25l_{\max}}\Delta l^{J} - \frac{11F_{\max}}{25(l_{\max})^{2}}\left(\Delta l^{J}\right)^{2} + \frac{48F_{\max}}{25(l_{\max})^{3}}\left(\Delta l^{J}\right)^{3} - \frac{16F_{\max}}{25(l_{\max})^{4}}\left(\Delta l^{J}\right)^{4}\right) = 0. \tag{10}$$

According to Equation (10), its expression form is characterized by a more complex nonintegrable term $\left(l^{J}+j\right)\dot{\theta}^{2}$ compared with the SLIP model. This leads to the result that the exact analytic solution does not exist and the mathematical expression is more complex as well.

Hence, considering the difficulty of utilizing the direct analytical method to solve the dynamic equation of the model, we employ the numerical simulation analysis method to address this issue.

3. Numerical simulation analysis of the QIPJCS model

3.1. SFA (step-to-fall analysis) numerical simulation analysis

For the stability of SLIP model, a large number of researchers have conducted related research works. The step-to-fall analysis (SFA) method was first presented by Seyfarth et al. in the literature [30]: this method is an effective numerical simulation method that aims at

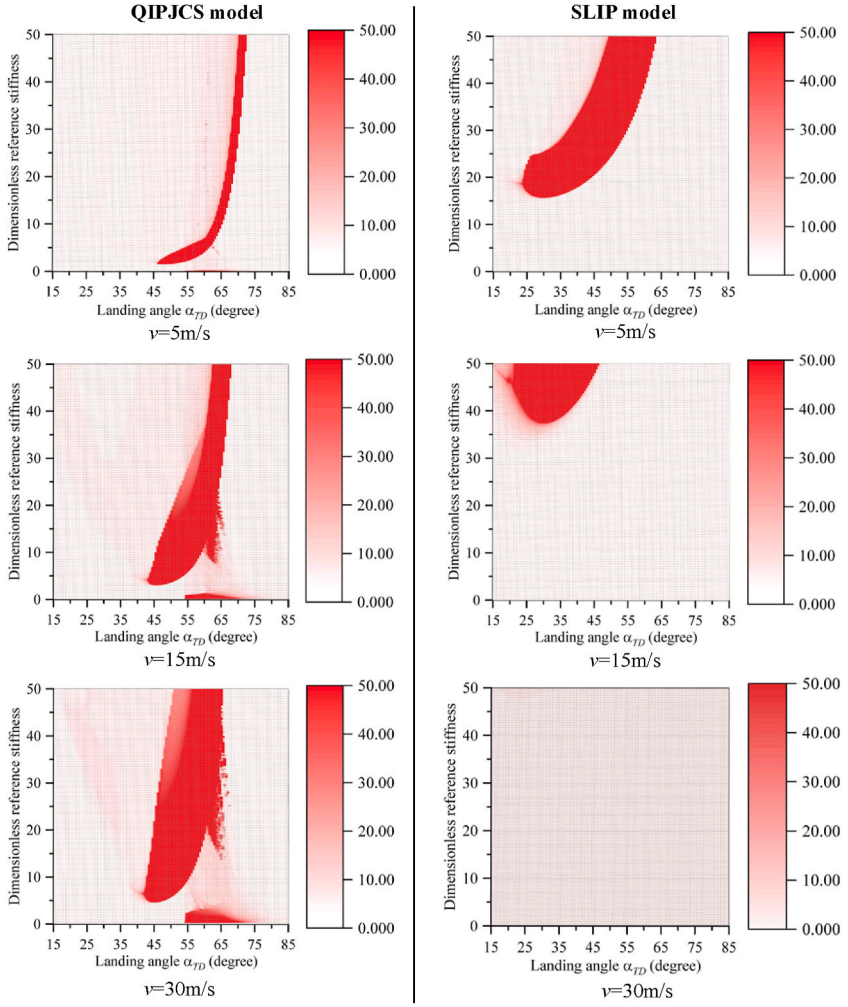

Fig. 5. The stable motion regions of the QIPJCS model (left column) and SLIP model (right column) for different given initial apex velocities ($v = 5$ m/s, $v = 15$ m/s, $v = 30$ m/s) with respect to allocation of the values of the landing angle (α_{TD}) and dimensionless reference stiffness ($\widetilde{k}_{10\%}$).

the case of a complex analytical expression of dynamics. Wróblewska et al. presented an analytical approximation of a reduced mapping which can be able to explicitly control the error of the approximation [31,32]. For the SFA method of classic SLIP model, the parameter set of $\{k, \alpha_{TD}, E_{sys}, m, l_0^S\}$ can determine the dynamics system. k is the stiffness coefficient of the linear spring, α_{TD} is the landing angle, E_{sys} is the energy of the system, m is the mass of the system, and l_0^S is the rest length of the linear spring. Moreover, E_{sys} is only related to the initial velocity at the apex (v) and initial height of the apex (y_a). Hence, the parameter set can be indicated as $\{k, \alpha_{TD}, v, y_a, m, l_0^S\}$. In general, m, l_0^S and y_a are set to constant for convenient discussion. Therefore, the SFA method is a solution based on the different allocations of set $\{k, \alpha_{TD}, v\}$ and calculates the gait cycle number N, which can satisfy completely passive and stable jumping motion. Three cases may occur during the motion process. To prevent infinite loops and excessively long simulation time, the gait cycle number of the simulation should be less than a threshold N_{max}. In this paper, $N_{max} = 50$.

Similar to the parameter set of the SLIP model, the dynamics system of the QIPJCS model can be determined by a parameter set as well. In particular, compared with k of the linear spring, the stiffness coefficient of the "J" curve spring is determined by Equation (2).

Thus far, the constant parameters of the SLIP and QIPJCS models can be given.

(1) Mass of system: $m = 80$kg;
(2) The rest length of the linear spring in the SLIP model is $l_0^S = 1$m, the rest length of the "J" curve spring in the QIPJCS model is $l_0^J = 0.5$m and the length of the rigid link in the QIPJCS model is $j = 0.5$m;
(3) The initial apex height: $y_a = 1$m.

For the convenience of discussion, the stiffness coefficients of the SLIP and QIPJCS models should be nondimensionalized. Based on the literature [18], the concept of dimensionless reference stiffness is utilized:

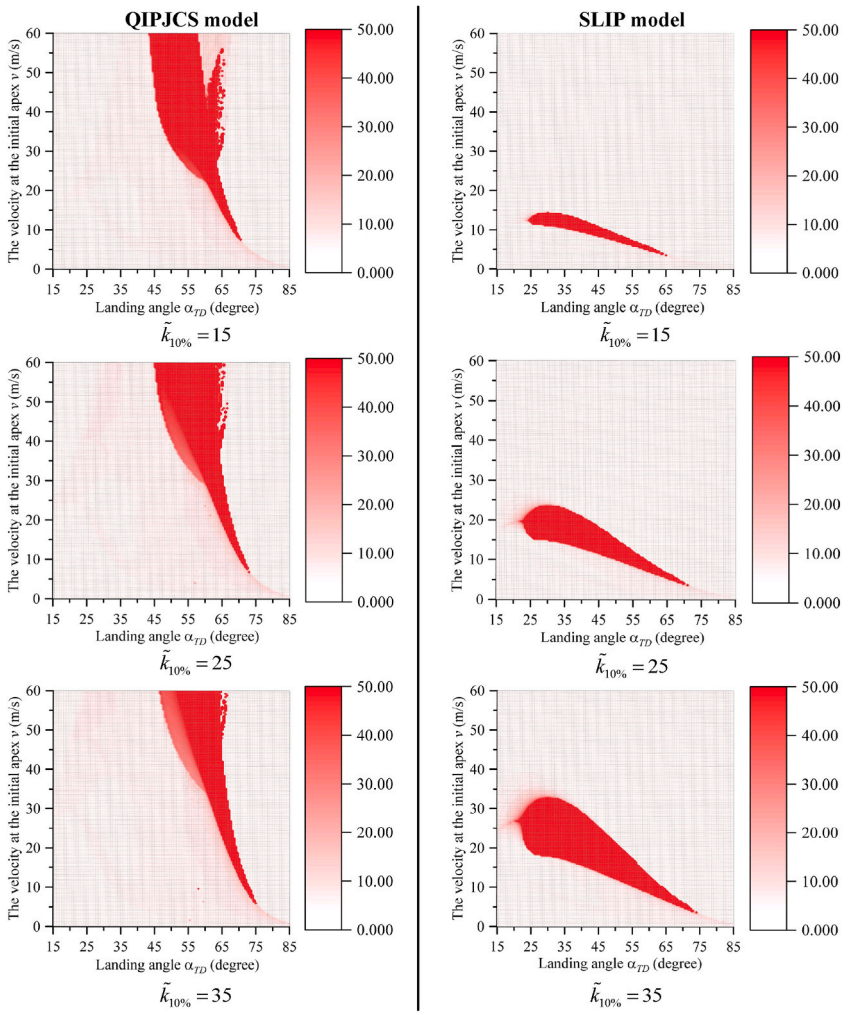

Fig. 6. The stable motion regions of the QIPJCS model (left column) and SLIP model (right column) for different given dimensionless reference stiffness values ($\tilde{k}_{10\%} = 15$, $\tilde{k}_{10\%} = 25$, $\tilde{k}_{10\%} = 35$) with allocation of the values of the landing angle (α_{TD}) and initial apex velocity (v).

$$\widetilde{k}_{10\%} = \frac{k_{10\%} l_0}{mg}, \tag{11}$$

where $k_{10\%}$ is the reference stiffness, which corresponds to the case of 10 % compression of the rest spring length.

Hence, the allocation of set $\{k, \alpha_{TD}, v\}$ can be equivalent to that of set $\{\widetilde{k}_{10\%}, \alpha_{TD}, v\}$. For the equivalent set, one parameter should be kept unchanged, and the remaining two parameters are allocated different values. After programming in MATLAB, the numerical simulation method is accomplished for analyzing the motion ability.

First, the stable motion regions of the QIPJCS model and SLIP model are analyzed by allocating the values of the landing angle (α_{TD}) and dimensionless reference stiffness ($\widetilde{k}_{10\%}$) at different given initial apex velocities (v). For the selection of the initial apex velocity, the high-speed reference value of v is 30 m/s. The reference values of v under low speed and moderate speed are selected as 5 m/s and 15 m/s, respectively.

As shown in Fig. 5, the entire stable motion region of the QIPJCS model increases with the increase in the given initial apex velocity v, and the overall shape of the stable motion region is presented as a "J".

Compared with the QIPJCS model, the whole stable motion region of the SLIP model decreases with the increase in the given initial apex velocity v, and the overall shape of the stable motion region is presented as a "J" at low speed. Moreover, the stable region of the SLIP model tends to have a dense distribution at moderate speed and vanishes at high speed. In the case of low speed ($v = 5$ m/s), the stable motion region of the SLIP model is superior to that of the QIPJCS model. In the case of moderate speed ($v = 15$ m/s), the stable motion regions of the two models are greatly different. The stable motion region of the SLIP model represents a high sensitivity with respect to stiffness and only exists in the range of stiffness from 34 to 50. No stable region exists under low stiffness. In contrast, the QIPJCS model can realize stable motion with a stiffness that ranges from 6 to 50. This phenomenon indicates that when the initial apex velocity v further increases, the stable motion region of SLIP will be further reduced within a limited range of stiffness, and finally, no

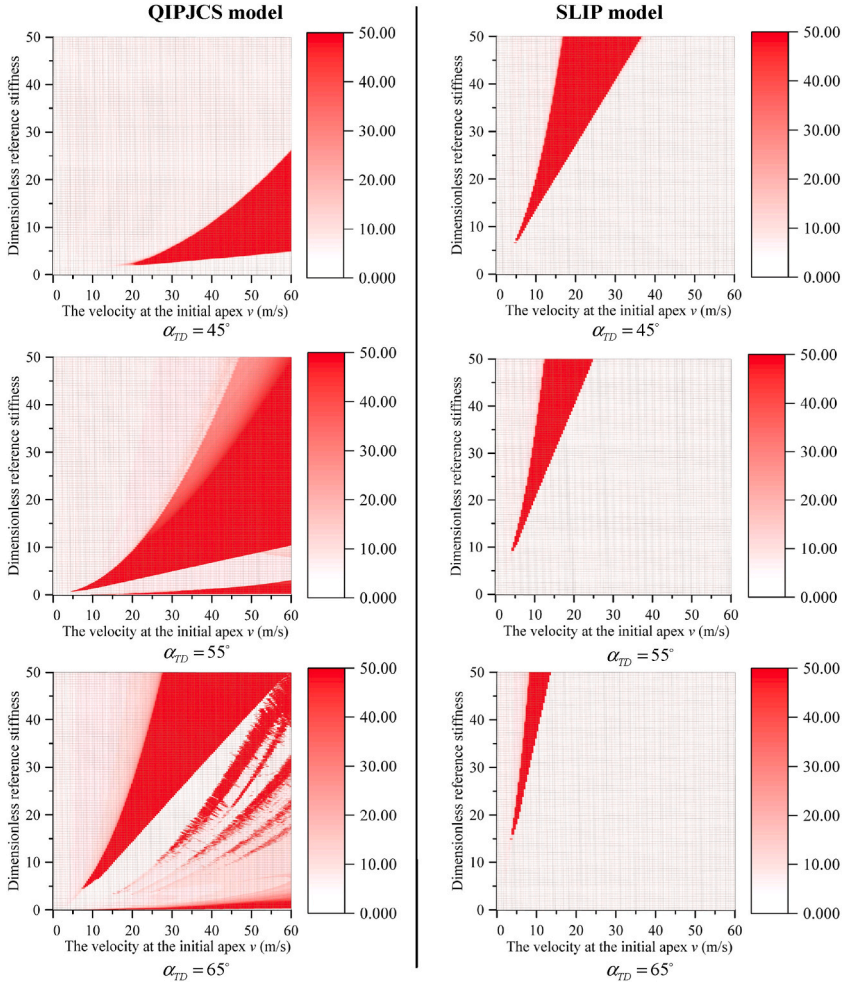

Fig. 7. The stable motion regions of the QIPJCS model (left column) and SLIP model (right column) for different given landing angle values ($\alpha_{TD} = 45^{\circ}$, $\alpha_{TD} = 55^{\circ}$, $\alpha_{TD} = 65^{\circ}$) with allocation of the initial apex velocity (v) and dimensionless reference stiffness ($\widetilde{k}_{10\%}$).

region can satisfy the stable motion condition. Meanwhile, due to the lower inferior limit of the stable motion region of the QIPJCS model, this model can continuously satisfy a certain stable motion within a limited range of stiffness. Namely, both models have a minimum stiffness limit for the range of stable motion, and this limit has less effect on the QIPJCS model compared with the SLIP model. In the case of high speed ($v = 30$ m/s), as mentioned above, the SLIP model cannot satisfy the requirements of stable motion within the given range of stiffness and landing angle. Meanwhile, the QIPJCS model can satisfy a certain stable motion in the range of stiffness values from 9 to 50. We also notice that the range of landing angles that can satisfy the stable motion of the QIPJCS model remains approximately unchanged at low, moderate and high speeds in the case of high stiffness. Meanwhile, in the case of high stiffness, the range of the landing angle that can satisfy the stable motion of the SLIP model only remains approximately unchanged at low speed (5 m/s). When the SLIP model moves with moderate speed (15 m/s), the range of landing angles that can satisfy the stable motion only increases with increasing stiffness.

Then, we discuss the stable motion region of the two models by allocating the values of the landing angle (α_{TD}) and initial apex velocity (v) under different dimensionless reference stiffnesses ($\widetilde{k}_{10\%}$).

As shown in Fig. 6, the whole stable motion region of the QIPJCS model changes slightly with the increase in the given dimensionless reference stiffness ($\widetilde{k}_{10\%}$) (left column), and the shape of the regions resembles a "J", which is mirrored. The whole stable motion region of the SLIP model increases with the increase in the given dimensionless reference stiffness ($\widetilde{k}_{10\%}$) (right column); meanwhile, in the case of the same dimensionless reference stiffness, the range of the landing angles that can satisfy the stable motion increases first and then decreases with the increase in the initial apex velocity (v). For instance, in the case of $\widetilde{k}_{10\%} = 25$, the stable motion region of the SLIP model increases constantly until the initial apex velocity (v) increases to 15 m/s. When the initial apex velocity (v) is greater than 15 m/s, the stable motion region decreases with increasing velocity. Moreover, the velocity allocation of the SLIP model that satisfies stable motion is restricted with a superior limit. For example, when $\widetilde{k}_{10\%} = 15$ and $\widetilde{k}_{10\%} = 25$, the superior limits are approximately 14 m/s and 23 m/s, respectively, and the superior limit is proportional to the given stiffness. This phenomenon indicates that if the SLIP model could maintain stable motion in the case of high initial apex velocity, the model stiffness needs to be further increased. The inferior limit of velocity that satisfies stable motion for all three stiffness cases is approximately 4 m/s. Correspondingly, the initial apex velocity superior limits of the QIPJCS model that satisfy stable motion in the three stiffness cases are greater than the given maximum speed limit, and the inferior limits are both approximately 6 m/s. The above analysis further indicates that the QIPJCS model is more suitable for stable motion with higher speed than the SLIP model.

Lastly, the stable motion regions of these two models should be discussed by allocating the initial apex velocity (v) and dimensionless reference stiffness ($\widetilde{k}_{10\%}$) under different given landing angles (α_{TD}).

As shown in Fig. 7, the whole stable motion region of the SLIP model decreases with increasing landing angle (right column). For the QIPJCS model (left column), the relationship between the change in the whole stable motion region and the change in the landing angle is not linear. Moreover, when the landing angle increases to 65°, the range of the stable motion region presents a certain discrete distribution. In this case of parameter allocation, the stable motion region of the QIPJCS model is superior to that of the SLIP model. Both models are limited with a minimum stiffness for the stable motion, and this minimum stiffness limit increases along with the given landing angle. Moreover, in the case of the same landing angle, the minimum stiffness limit of the QIPJCS model is smaller than that of the SLIP model. For instance, in the case of $\alpha_{TD} = 45°$, the respective minimum stiffness limits of the QIPJCS model and SLIP model which can satisfy the stable motion are approximately 2 and 9. In addition, this difference is even more significant when the landing angle increases. For the SLIP model, the whole stable motion region is mainly distributed in the low- and moderate-speed motion areas. The SLIP model can barely satisfy stable motion at high speed. Moreover, the maximum initial apex velocity that can satisfy stable motion will decrease with the increase in the given landing angle. For instance, in the case of $\alpha_{TD} = 45°$, the maximum initial apex velocity is limited to approximately 38 m/s. When the landing angle increases to 65°, the maximum initial apex velocity decreases to 13 m/s. For the QIPJCS model, the whole stable motion region is mainly distributed in the high-speed motion area. In these three landing angle cases, the model can ensure a certain stable motion. Moreover, when the given landing angle increases, the stable motion regions at low and moderate speeds increase to a certain degree. Hence, the QIPJCS model is more suitable for stable motion at high speed but can still ensure certain stable motion at low and moderate speeds.

According to the above three different parameter allocation analyses, compared with the SLIP model, the minimum stiffness limit of the QIPJCS model, which can realize stable motion, is smaller (lower stiffness sensitivity). Moreover, the QIPJCS model possesses a higher stable motion speed. All of the analyses indicate that the QIPJCS model is a better biological stiffness model for stable motion, especially in the case of high speed.

3.2. ARM (Apex-Return-Map) numerical simulation analysis

The SFA numerical simulation method can neither detect the self-stability of the model after the threshold value nor ensure the correctness of the detection results by increasing the threshold value. Therefore, scholars presented a numerical simulation method called ARM (Apex-Return-Map) to study the self-stability of the SLIP model. This section employs this method to further analyze the motion performance of the QIPJCS model.

3.2.1. The building of ARM of the QIPJCS model

When a system degenerates from the vector field space to a one-dimensional scalar system, the Poincaré map of this system can be converted into a special form called a return map. Hence, to conveniently conduct the dynamic analysis of a system with a periodic

trajectory, the Poincaré map can be transformed into the return map with a simpler expression.

In general, as shown in Fig. 8, a complete gait cycle i of the QIPJCS model can be divided into the following parts, similar to the SLIP model.

(1) The apex state of the flight phase is $\boldsymbol{C}_i := (y_{ai}, v_i)^T$;
(2) The falling stage of flight phase *FD*;
(3) The moment of touchdown *TD*;
(4) The stance phase *ST*;
(5) The moment of leaving the ground *LO*;
(6) The surface disconnection stage of the flight phase *FU*.

Afterward, the model enters the next gait cycle i+1, and the apex state of the flight phase is $\boldsymbol{C}_{i+1} := (y_{ai+1}, v_{i+1})^T$. Then, the apex return map can be defined as $\boldsymbol{C}_{i+1} = P_{ARM}(\boldsymbol{C}_i)$, where $\boldsymbol{C}_i$ and $\boldsymbol{C}_{i+1}$ belong to Q_a and Q_a is a simply connected open set in $\mathbb{R}^2$. Moreover, the motion sketch of the QIPJCS model during a complete gait cycle is shown in Fig. 9, and the reference coordinate system is defined as $\{O\}$. Hence, the motion characteristics of the apex return map in different stages of the complete gait cycle can be analyzed as follows.

First, the total energy of the model is given. The velocity of the apex along the x-axis in gait cycle i can be represented as v_i, and the velocity of the apex along the y-axis is obviously 0. The height, which is relative to the reference coordinate system $\{O\}$, is denoted as y_{ai}. In this stage, the model is only affected by gravity, and the energy of the system is conserved according to Hypothesis 2 in Section 2.2. Therefore, the apex velocity of the whole system in gait cycle i can be expressed as:

$$v_i = \sqrt{2\left(E_{sys} - mgy_{ai}\right)/m}. \tag{12}$$

Then, the apex state of the flight phase of current gait cycle i is:

$$\boldsymbol{C}_i := (y_{ai}, v_i)^T = \begin{bmatrix} y_{ai} \\ \sqrt{2\left(E_{sys} - mgy_{ai}\right)/m} \end{bmatrix}. \tag{13}$$

The process of movement from the *Apex* of gait cycle i to the moment of touchdown *TD* is a submap of ARM P_{ARM}, and this submap can be denoted as P_{FD}.

(b) The moment of touchdown *TD*

The moment of touchdown is the transition between the falling stage and stance phase. The switch critical condition of this moment is:

$$y = y_{TD} = s_0 \sin \alpha_{TD} = \left(l_0' + j\right)\sin \alpha_{TD}. \tag{14}$$

The state of *TD* is defined as $\boldsymbol{q}_{TD}^i$, and $\boldsymbol{q}_{TD}^i$ satisfies:

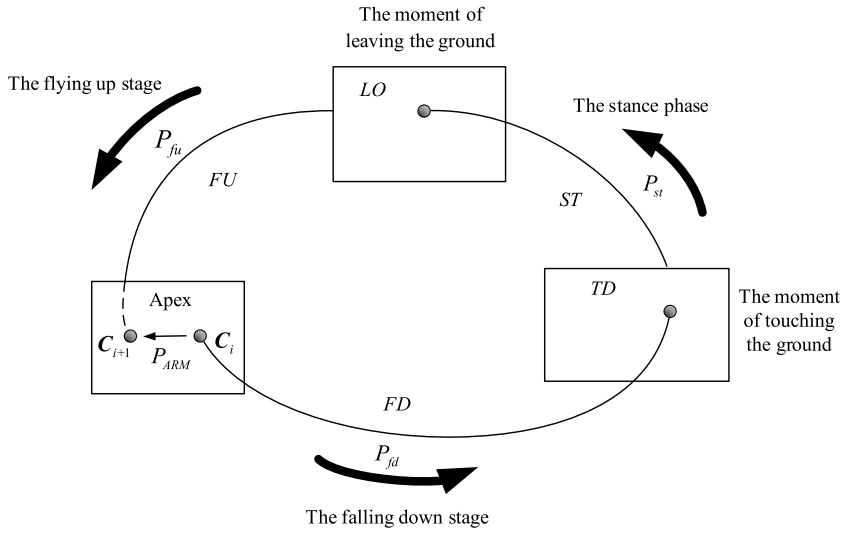

Fig. 8. The ARM of the QIPJCS model during a complete gait cycle.

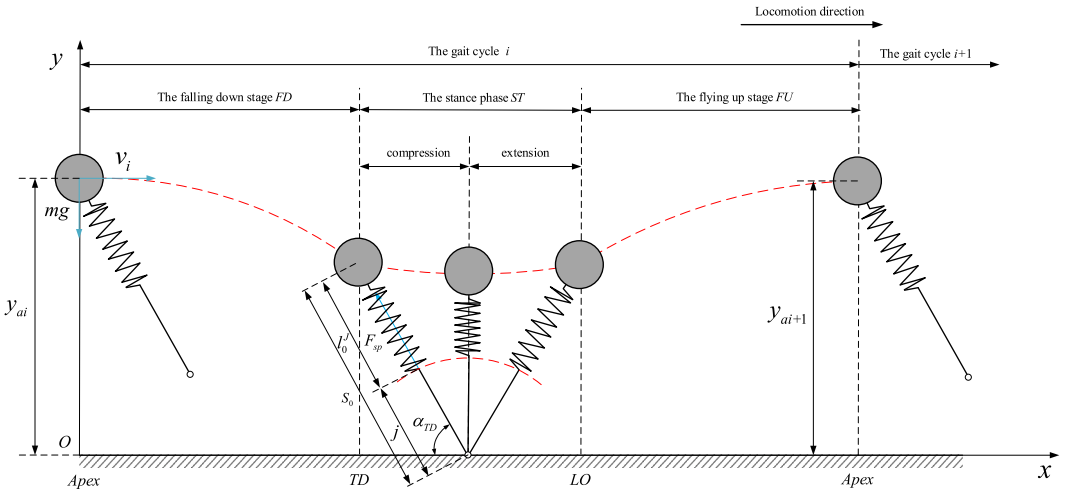

Fig. 9. The motion sketch of the QIPJCS model during a complete gait cycle.
(a) The falling stage of flight phase *FD*.

$$\boldsymbol{q}_{TD}^{i}=\begin{bmatrix} x_{TD} \\ \dot{x}_{TD} \\ y_{TD} \\ \dot{y}_{TD} \end{bmatrix}=\begin{bmatrix} \dot{x}_{TD}\sqrt{2(y_{ai}-y_{TD})/g} \\ v_i \\ (l_0^J+j)\sin\alpha_{TD} \\ -\sqrt{2g(y_{ai}-y_{TD})} \end{bmatrix}=\begin{bmatrix} \sqrt{4(E_{sys}-mgy_{ai})(y_{ai}-(l_0^J+j)\sin\alpha_{TD})/mg} \\ \sqrt{2(E_{sys}-mgy_{ai})/m} \\ (l_0^J+j)\sin\alpha_{TD} \\ -\sqrt{2g(y_{ai}-(l_0^J+j)\sin\alpha_{TD})} \end{bmatrix}, \tag{15}$$

where x_{TD} denotes the distance between the mass point m and the origin of coordinate system $\{O\}$ along the x-axis at TD, $\dot{x}_{TD}$ denotes the velocity of m in $\{O\}$ along the x-axis, y_{TD} denotes the distance between m and the origin of $\{O\}$ along the y-axis at TD, and $\dot{y}_{TD}$ denotes the velocity of m in $\{O\}$ along the y-axis.

(c) The stance phase *ST*

After touchdown, the model enters stance phase *ST* from the falling stage. *ST* can be divided into two stages according to the compression or tension of the model spring: in the compression process, the J-curve spring of the QIPJCS model transitions from the initial length state to the maximum compression state and stores the elastic potential energy; in the tension process, the spring transitions from the maximum compression state to the initial length state and releases the elastic potential energy.

Compared with the flight phase, the model is affected not only by gravity but also by the support force from the ground. Meanwhile, the support force can be denoted as F_{spr}, which is the elastic force of the spring. The motion equations are determined as follows:

$$\begin{cases} m\ddot{x}_{ST}=F_{spr}\dfrac{x_{ST}-x_{FP}}{\sqrt{(x_{ST}-x_{FP})^2+(y_{ST}-y_{FP})^2}} \\ m\ddot{y}_{ST}=F_{spr}\dfrac{y_{ST}-y_{FP}}{\sqrt{(x_{ST}-x_{FP})^2+(y_{ST}-y_{FP})^2}}-mg \end{cases}, \tag{16}$$

where x_{ST} denotes the distance between the projection of m on the x-axis and the origin of $\{O\}$ during *ST*, y_{ST} denotes the distance between the projection of m on the y-axis and the origin of $\{O\}$ during *ST*, x_{FP} denotes the coordinate of the projection of the foothold on the x-axis in $\{O\}$ during *ST*, and y_{FP} denotes the coordinate of the projection of the foothold on the y-axis in $\{O\}$ and $y_{FP}=0$ during *ST*.

The process that occurs from the moment of touchdown *TD* to the moment of leaving the ground *LO* is a submap of ARM P_{ARM} as well: P_{ST}.

(d) The moment of leaving the ground *LO*

The moment of leaving the ground represents the transition between the stance phase and the surface disconnection stage. The switch critical condition of this moment is:

$$s = s_0 = l_0^J + j. \tag{17}$$

Equation (17) can also be employed as the switch critical condition of *TD*. For the projections of *m* on the *x*- and *y*-axes at *LO*, x_{LO} and y_{LO} can be determined by the step-by-step integration numerical method. The step size of integration is set as $\Delta t_n = 10^{-4}(n = 1,2,3\cdots)$, and the calculation process is shown in Fig. 10.

After *LO*, the foothold of the model leaves the ground and enters *FU*. During this stage, part of the kinetic energy of the system is converted to gravitational potential energy until the velocity along the *y*-axis is 0. Meanwhile, when the model reaches the *Apex* of gait cycle i+1, the model has accomplished a complete gait cycle and enters the next gait cycle. The submap of ARM that moves from *LO* to the *Apex* of gait cycle i+1 can be defined as P_{FU}.

During *FU*, the system is only affected by gravity; hence, the apex state of the flight phase of the next gait cycle i+1 is:

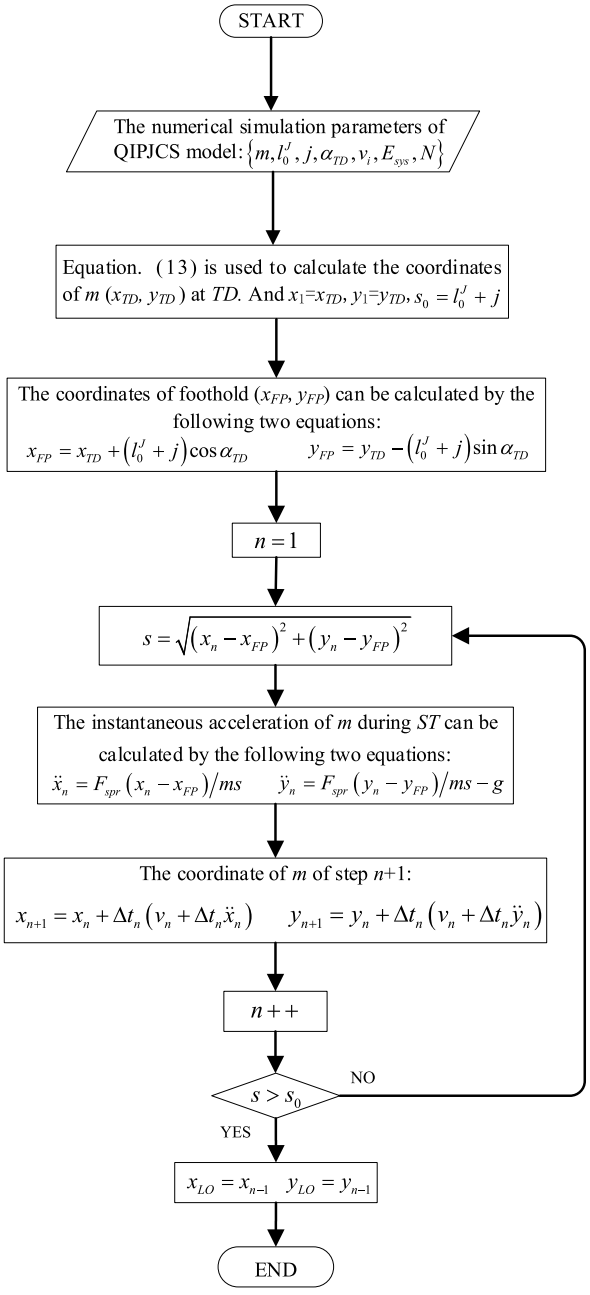

Fig. 10. The calculation process of the coordinates of *m* at *LO*.
(e) The surface disconnection stage of the flight phase *FU*.

$$\boldsymbol{C}_{i+1} : = (y_{ai+1}, v_{i+1})^T = \begin{bmatrix} y_{LO} + \frac{1}{2g}\dot{y}_{LO}^2 \\ \dot{x}_{LO} \end{bmatrix}, \tag{18}$$

where y_{LO} denotes the coordinate of m on the y-axis at LO, $\dot{y}_{LO}$ denotes the velocity component along y of m during FU, and $\dot{x}_{LO}$ denotes the velocity component along x of m during FU.

In conclusion, the ARM that presents gait cycle i to gait cycle i+1 $\boldsymbol{C}_{i+1} = P_{ARM}(\boldsymbol{C}_i)$ can be determined:

$$P_{ARM} : \boldsymbol{C}_i : = \begin{bmatrix} y_{ai} \\ v_i \end{bmatrix} = \begin{bmatrix} y_{ai} \\ \sqrt{2\left(E_{sys} - mgy_{ai}\right)/m} \end{bmatrix} \to \begin{bmatrix} y_{ai+1} \\ v_{i+1} \end{bmatrix} = \begin{bmatrix} y_{LO} + \frac{1}{2g}\dot{y}_{LO}^2 \\ \dot{x}_{LO} \end{bmatrix} : = \boldsymbol{C}_{i+1}. \tag{19}$$

Moreover, P_{ARM} can be denoted as the composition of three submaps:

$$P_{ARM} = P_{FD} \circ P_{ST} \circ P_{FU} : \boldsymbol{C}_i \to \boldsymbol{C}_{i+1}. \tag{20}$$

3.2.2. Fixed point analysis of the QIPJCS model

In this paper, the motion space of the stable motion of the QIPJCS model can also form a periodic closed orbit like the SLIP model. For the ARM with dimension reduced to one, the periodic closed orbit can be represented as the fixed point on the Poincaré section.

The fixed point can be defined as follows: the ARM of the system is given as P_{ARM} and $\boldsymbol{C}_{i+1} = P_{ARM}(\boldsymbol{C}_i)$. If and only if the state of one point in a gait cycle ($\boldsymbol{C}^*$) satisfies $\boldsymbol{C}^* = P_{ARM}(\boldsymbol{C}^*)$, then $\boldsymbol{C}^*$ is the fixed point of ARM P_{ARM}. According to Hypothesis 2, the mechanical energy is conserved during a gait cycle; hence, the state of apex $\boldsymbol{C}^*$ can be represented by an apex height of m in gait cycle i (y_{ai}) or an apex velocity of m in gait cycle i (v_i). Compared with v_i, y_{ai} is more visualized and easier to sketch. Therefore, y_{ai} is selected as the reference variable, and $\boldsymbol{C}_{i+1} = P_{ARM}(\boldsymbol{C}_i)$ can be denoted as a map with one dimension:

$$y_{ai+1} = P_{ARM}(y_{ai}). \tag{21}$$

Similarly, the fixed point $\boldsymbol{C}^*$ should satisfy:

$$y^* = P_{ARM}(y^*). \tag{22}$$

Based on Equations (21) and (22), the fixed point can be denoted as $y^* = y_{ai+1} = y_{ai}$.

Referring to Ref. [18], the stability criteria of the fixed point of the QIPJCS model are the same as those of the SLIP model:

$$\sigma = \left.\frac{dy_{ai+1}}{dy_{ai}}\right|_{y^*}. \tag{23}$$

A sketch of the fixed point during gait cycle i is shown in Fig. 11, and the range of the stable motion region is:

$$|\sigma| < 1, \tag{24}$$

$$-1 < \left.\frac{dy_{ai+1}}{dy_{ai}}\right|_{y^*} < 1. \tag{25}$$

According to Equation (25), when the absolute value of the slope of $y_{ai+1} = P_{ARM}(y_{ai})$ at $y_{ai} = y^*$ is less than 1, y^* is the stable fixed

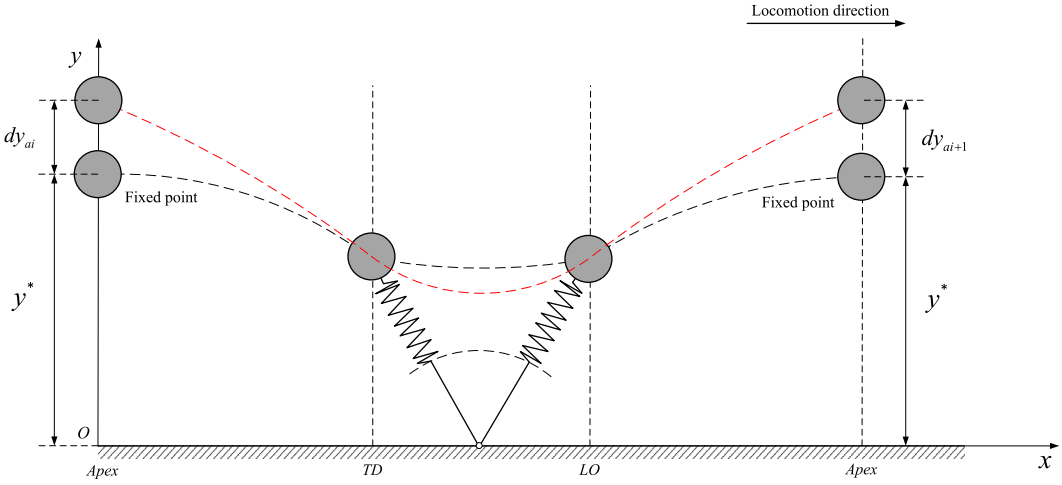

Fig. 11. Sketch of a fixed point during gait cycle i.

point of the system; otherwise, when the absolute value of the slope at $y_{ai} = y^*$ is greater than 1, y^* is the unstable fixed point.

Employing the numerical simulation method presented in Section. 3.2.1, the fixed point of ARM of the QIPJCS model is analyzed. For the analysis of the neighborhood at a fixed point, the slope of the ARM curve represents the dynamic performance of the neighborhood. First, the constant parameters of the numerical simulation analysis are given as follows.

(1) Mass of system: $m = 80$kg;
(2) The rest length of the "J" curve spring l_0^J is 0.5 m, and the length of rigid link j is 0.5 m;
(3) The total energy of the system is $E_{sys} = 9784.8$J. In other words, the initial apex height and the initial apex velocity are $y_a = 1$m and $v = 15$m/s, respectively;

Then, the effects of the stiffness and landing angle on the fixed point of the QIPJCS model are investigated as follows.

(a) The effects of different reference stiffnesses on fixed points

First, the same landing angle is set as 65°, and the ARM curves with different reference stiffnesses ($k_{10\%} = 15696$N/m, $k_{10\%} = 23544$N/m and $k_{10\%} = 31392$N/m) are determined by numerical simulation, as shown in Fig. 12. All three ARM curves intersect the diagonal line with only one point within the given height of motion, and all the slopes at these points are less than 1. Hence, these intersection points are the stable fixed points of the QIPJCS model under three different reference stiffnesses. All initial apex height conditions in the neighborhood of these points can make the model system converge to stable periodic motion. Moreover, with the increase in the reference stiffness, the value of the stable fixed point and the slope at the fixed point increase as well. As a result, the basis of attraction decreases [33].

First, the same reference stiffness is set as 7848 N/m, and the ARM curves with different landing angles ($\alpha_{TD} = 50°$, $\alpha_{TD} = 53°$ and $\alpha_{TD} = 56°$) are determined by numerical simulation, as shown in Fig. 13. In the case of $\alpha_{TD} = 50°$, the ARM curve intersects the diagonal line with two points. The slope of the point with a lower position is less than 1; hence, this point is the fixed point. The slope of the other point is greater than 1, and this point is the unstable fixed point. For the two remaining cases, the ARM curves intersect the diagonal line with only one point (fixed point) within the given height of motion. With the increase in the landing angle, the value of the stable fixed point and the slope at the fixed point decrease. As a result, the basin of attraction grows. For the unstable fixed point of $\alpha_{TD} = 50°$, any subsequent initial apex height condition cannot make the model system converge to stable periodic motion, and the model system will diverge to the unstable state after limited cycles.

From the above simulation results, the oversize reference stiffness and the undersize landing angle will cause the ARM curve of the model to gradually deviate from the diagonal line. Therefore, no stable fixed point exists, and the model system diverges. The stable periodic motion of the model cannot be realized.

The investigation of the slope of the ARM curve directly reflects the number of gait cycles that guarantees that the model system can converge to stable periodic motion or diverge to the unstable state. The dynamic performance of the model in the neighborhood of one point can be known by analyzing the slope of the curve at this point. As the slope of the ARM curve approaches 0, the sensitivity of the model system to the initial value of motion becomes lower, and the model system can converge to stable periodic motion faster. In contrast, as the slope of the ARM curve approaches 1, the sensitivity of the model system to the initial value of motion is higher, and the number of gait cycles that makes the model system converge to stable periodic motion is added. Even the model system gradually diverges to the unstable state.

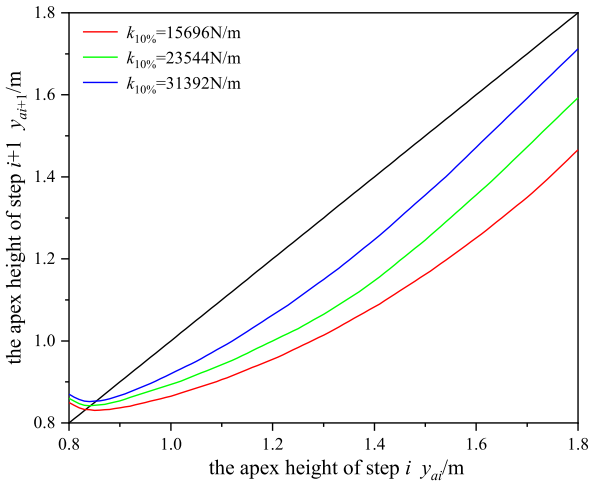

Fig. 12. The effects of different reference stiffnesses on the fixed point.
(b) The effects of different landing angles on fixed points.

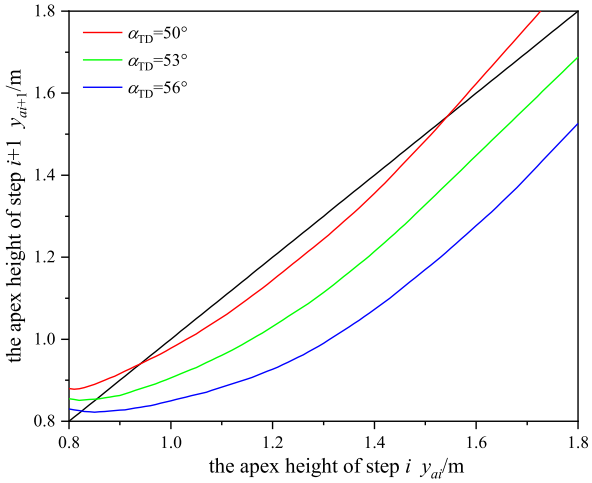

Fig. 13. The effect of the landing angle on a fixed point.

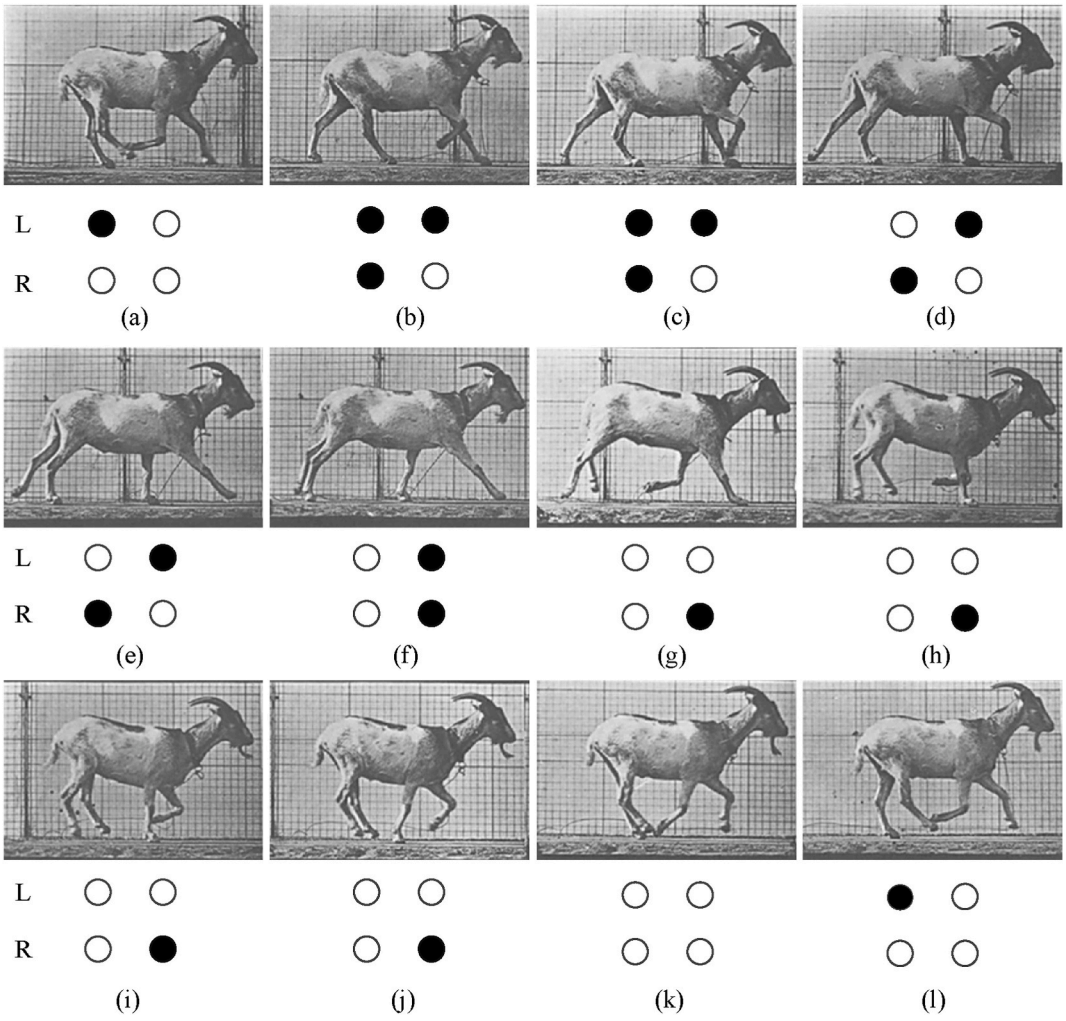

Fig. 14. Sketch of a gait cycle of goat galloping and the corresponding hoof points.

4. Inherent running mechanism analysis of goat natural gait

Based on the analysis of the QIPJCS model, which is equivalent to the single goat limb and the goat gait in the natural environment, the motion characteristics of all goat limbs can be investigated during a gait cycle, and the inherent running mechanism of coordinated motion in quadruped mammal limbs with natural gait can be further revealed. Goats can employ different gaits according to different environments during the walking motion. Moreover, natural gaits can be divided into six types depending on the differences in stride length and frequency: walk, trot, pace, gallop, canter and bound [34]. In general, the velocity of gallops is the maximum among the natural gaits of large quadruped mammals (such as ruminants) because the stride length of gallops is the maximum. The main characteristic of galloping is that four hoof beats exist in a gait cycle. Moreover, the stride length of diagonal limbs increases because of the high velocity, and two front hooves and two hind hooves land on the ground almost at the same time. Hence, in a gait cycle, the number of hoof beats can be approximately counted as two. In this paper, galloping is selected to analyze the running mechanism of quadruped mammals. A sketch of a gait cycle of goat galloping and the corresponding hoof points is shown in Fig. 14.

According to the keyframes of goat galloping in Fig. 14, the process of this type of gait is investigated: keyframe (a) is the initial state of a gallop gait cycle; at this moment, only LH (left hind limb) lands on the ground and one hoof beat exists; during keyframes (b)–(c), LF (left front limb) and RH (right hind limb) land on the ground as well, and three hoof beats exist; during keyframes (d)–(e), LH, which lands on the ground first, is left and the remaining two hoof beats belong to LF and RH; at keyframe (f), RF (right front limb) lands on the ground and RH is left at the same time, and two hoof beats exist (LF and RF); during keyframe (g)–(j), LF is left and the goat is only supported by RF, and hence, one hoof beat exists; keyframe (k) represents the flight phase and no hoof beat existing; at keyframe (l), LH lands on the ground again and one hoof beat exists, and the goat will enter the next gait cycle.

The equivalent mechanism can be built for each keyframe of the goat gallop based on the gait analysis, as shown in Fig. 15.

For keyframes (a)–(b), the knee joint, tarsometatarsal joint and metatarsophalangeal joint of the goat are on the same support line in the sagittal plane during the motion process, as shown in Fig. 16. Based on the theory of the dead-point support effect, the joint torque can be transformed into the structural torque of the bone under this configuration of joints. It is beneficial for the goat to buffer the motion impact that comes from the process of transitioning from the flight phase to the stance phase to retain stable motion. Moreover, the muscle group of the hip joint plays the main role of a buffer and energy store. Hence, for LH, this limb can be considered equivalent to a typical QIPJCS model. For RH and LF at keyframe (b), these two limbs land on the ground at the same time and form a floating support mechanism with a quasi quadrangle.

For keyframes (c)–(e), the most important characteristic of this process is the equivalent mechanism formed by the interaction between the goat and ground in the sagittal plane, as shown in Fig. 17. The state of LH at keyframe (c) represents the stretching stage of the stance phase and provides the forward momentum for goat galloping. Two links (RH and LF) of the equivalent mechanism are driven to rotate, and then the body of the goat can be pushed forward; for keyframes (d)–(e), LH is in flight, and then the forward movement of the goat body can be considered as approximately equivalent to the motion process of a four-link mechanism. Moreover, due to the physiological differences of limbs and the characteristics of gallops, a phase difference exists between the equivalent models of RH and LF. RH transitions to the flight phase first.

For keyframe (f), RH has already changed to the stance phase, and LF is in the stretching stage of the stance phase. Meanwhile, RF lands on the ground. The elbow joint, wrist joint and metacarpophalangeal joint of RH obey the theory of a dead-point support effect and are on the same support line. At every moment of keyframe (f), RF, LF and the ground form a triangular truss structure together, as

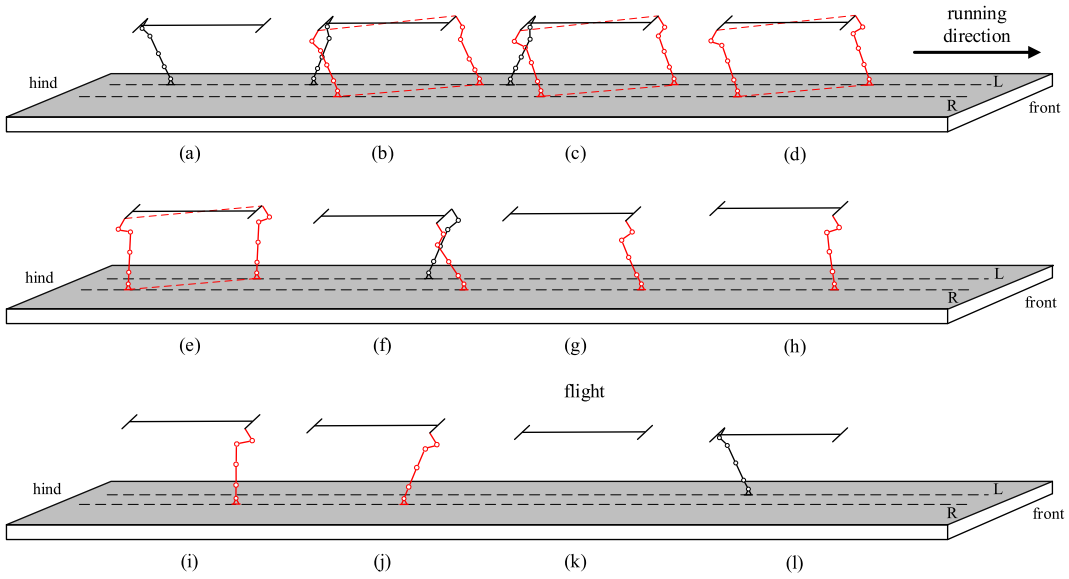

Fig. 15. The equivalent mechanism sketch of a gallop gait cycle.

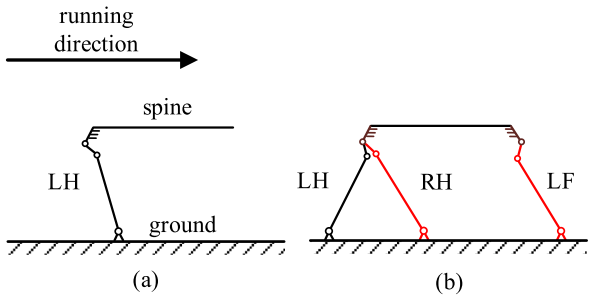

Fig. 16. The equivalent mechanism sketch of keyframes (a)–(b).

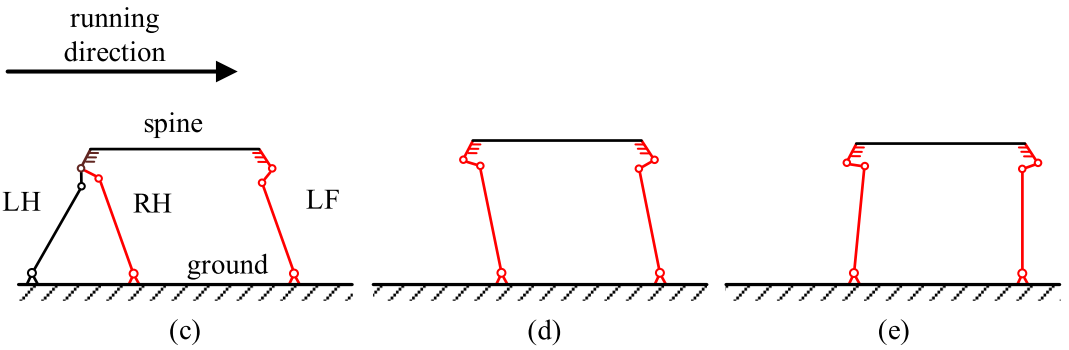

Fig. 17. The equivalent mechanism sketch of keyframes (c)–(e).

shown in Fig. 18. This structure is beneficial for stable support during goat galloping.

For keyframes (g)–(j), the goat only relies on RF to support the body during this process. RF can be considered equivalent to a typical QIPJCS model during this whole process, as shown in Fig. 19. The support line formed by the elbow joint, wrist joint and metacarpophalangeal joint on the RF is perpendicular to the ground, and the spring of the equivalent QIPJCS model is in the maximum compression state.

For keyframe (k), the four limbs of the goat have already transitioned to the flight phase.

For keyframe (l), LH lands on the ground again, and the state of LH is the same as in keyframe (a). Meanwhile, this keyframe is the start of the next gait cycle.

Based on the above analysis of the equivalent mechanism during the goat galloping process, the stance phase of the forelimb is selected as the representative to proceed with the force analysis of the dynamic motion of the goat, as shown in Fig. 20. The goat proceeds with uniformly accelerated motion, and the acceleration is $\boldsymbol{a}$.

The forelimb can be equivalent to a QIPJCS model. First, the shoulder joint is equivalent to the buffer elastic unit. According to the dead-point support effect, all joints are on the support line of the dead-point, and all the joint torques are 0 except for the elbow joint that provides the driving torque. The body of the goat is supported by structural torque. Hence, the parts below the elbow joint are

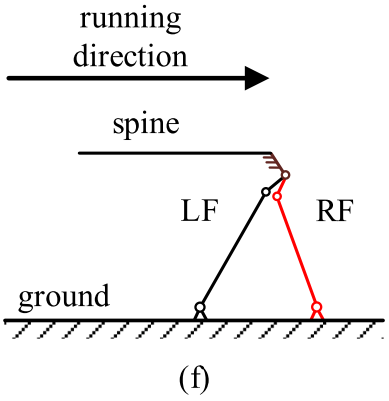

Fig. 18. The equivalent mechanism sketch of keyframe (f).

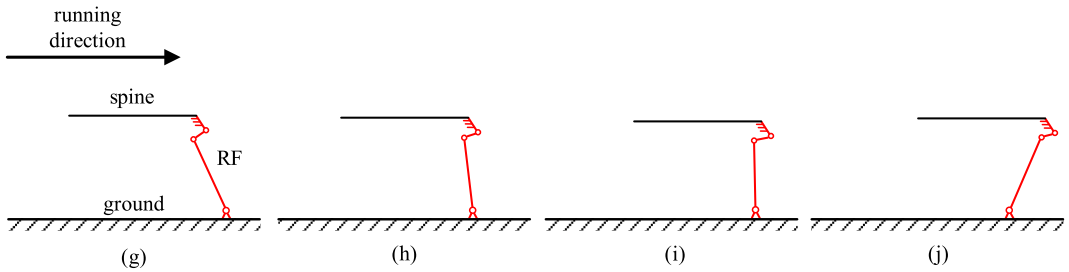

Fig. 19. The equivalent mechanism sketch of keyframes (g)–(j).

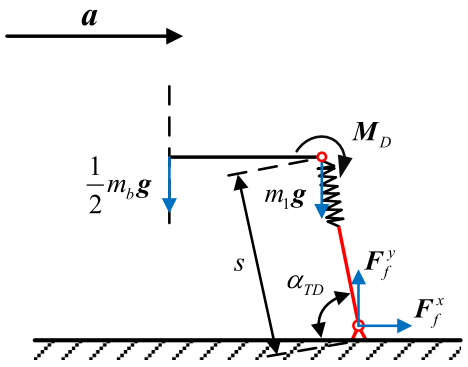

Fig. 20. Forecast analysis during the stance phase.

equivalent to a rigid link, and for the convenience of analysis, the shoulder joint and elbow joint are considered equivalent to a rotation joint to connect the body and the elastic unit.

The whole equivalent length of the forelimb is s; the angular acceleration of the equivalent joint can be denoted as:

$$\boldsymbol{\alpha} = \boldsymbol{a}s. \tag{26}$$

The total moment of the equivalent joint $\boldsymbol{M}_T$ is:

$$\boldsymbol{M}_T = I\boldsymbol{\alpha} = m_1 s^3 \boldsymbol{a}, \tag{27}$$

where I is the momentum of inertia of the forelimb equivalent mechanism with respect to the landing point and $I = m_1 s^2$, m_1 is the mass of forelimb.

According to Newton's second and third laws, the force analysis of the equivalent mechanism can be determined:

$$\boldsymbol{F}_f^x = \frac{1}{2}(m_1 + m_2 + m_b)\boldsymbol{a}, \tag{28}$$

$$\boldsymbol{F}_f^y = \left(m_1 + \frac{1}{2}m_b\right)\boldsymbol{g}, \tag{29}$$

where $\boldsymbol{F}_f^x$ and $\boldsymbol{F}_f^y$ are the component forces of the support force from the ground along the x-axis and y-axis, respectively, m_2 is the mass of the hindlimb, and m_b is the mass of the goat body.

Moreover, the total moment of the equivalent joint can be denoted as follows:

$$\boldsymbol{M}_T = \boldsymbol{M}_D + \boldsymbol{M}_f^x + \boldsymbol{M}_f^y + \boldsymbol{M}_b, \tag{30}$$

where $\boldsymbol{M}_D$ is the driving torque of the equivalent joint, $\boldsymbol{M}_f^x$ and $\boldsymbol{M}_f^y$ are the moments of $\boldsymbol{F}_f^x$ and $\boldsymbol{F}_f^y$ acting on the equivalent joint, and $\boldsymbol{M}_b$ is the moment of gravity of m_b acting on the equivalent joint.

In addition, each torque can be calculated as follows:

$$\boldsymbol{M}_f^x = \boldsymbol{F}_f^x s \sin \alpha_{TD}, \tag{31}$$

$$\boldsymbol{M}_f^y = \boldsymbol{F}_f^y s \cos \alpha_{TD}, \tag{32}$$

$$\boldsymbol{M}_b = \frac{1}{2} m_b \boldsymbol{g} s. \tag{33}$$

Based on Equations (27) and (30):

$$\boldsymbol{M}_D + \boldsymbol{M}_f^x + \boldsymbol{M}_f^y + \boldsymbol{M}_b = m_1 s^3 \boldsymbol{a}. \tag{34}$$

Equations (31)–(33) can be substituted into Equation (34), and the driving torque $\boldsymbol{M}_D$ can be calculated as follows:

$$\boldsymbol{M}_D = m_1 s^3 \boldsymbol{a} - \boldsymbol{F}_f^x s \sin \alpha_{TD} - \boldsymbol{F}_f^y s \cos \alpha_{TD} - \frac{1}{2} m_b \boldsymbol{g} s. \tag{35}$$

Then, Equations (28) and (29) can be substituted into Equation (35):

$$\boldsymbol{M}_D = m_1 s^3 \boldsymbol{a} - \frac{1}{2}(m_1 + m_2 + m_b)\boldsymbol{a} s \sin \alpha_{TD} - \left(m_1 + \frac{1}{2} m_b\right) \boldsymbol{g} s \cos \alpha_{TD} - \frac{1}{2} m_b \boldsymbol{g} s. \tag{36}$$

In consideration of the actual motion of a goat, the flexion and extension range of the shoulder joint of the goat forelimb, which is compared with the length of the whole limb, can be ignored. Hence, s can be regarded as constant. Moreover, due to m_1, m_2 and m_b are constant as well. Equation (36) can also be denoted as follows:

$$\boldsymbol{M}_D = m(\alpha_{TD}). \tag{37}$$

According to Equation (37), the driving torque of equivalent joint $\boldsymbol{M}_D$ is only affected by the landing angle α_{TD}. Therefore, in the case of stable goat motion with constant acceleration $\boldsymbol{a}$, the driving torque can be reduced for energy conservation by optimizing the landing angle within limits.

5. Conclusion

In this paper, the large mammal goat is chosen as the study object, and a novel bionic stiffness model is presented based on goat anatomy. The elastic unit of this model is equivalent to the flexion and extension muscles, tendons and other tissues of the goat shoulder joint. Hence, because of the nonlinear characteristic of these biological tissues, a nonlinear spring with a "J"-shaped force–deformation curve is utilized. The parts below the elbow joint can be considered equivalent to a rigid link based on the dead-point support effect. Finally, the combination of the nonlinear spring and the rigid link constitutes the QIPJCS model.

For the dynamic performance analysis of the QIPJCS model, the dynamics equations are derived first, and then we refer to the SFA numerical method. The simulation results of the QIPJCS model are compared with the classical SLIP model under three different cases by the reasonable allocation of parameter set $\{\widetilde{k}_{10\%}, \alpha_{TD}, v\}$. All three analysis results indicate that the QIPJCS model presented in this paper has a larger range of stable motion than the SLIP model and achieves a better dynamic performance. For the motion performance of the model beyond the simulation threshold, the ARM of the QIPJSC model is established. Based on this ARM, the sensitivity of the model fixed point to parameter variation is investigated by numerical simulation. The results indicate that an excessively large or small reference stiffness and landing angle will result in the divergence of the system and the loss of stabilization of the model.

Afterward, according to the motion process of a typical goat natural gait (gallop), the keyframes of a complete gait cycle are extracted, and then the equivalent mechanisms of all keyframes in the sagittal plane are established. Moreover, the gait sequences can be classified based on the equivalent mechanism state. Each limb obeys the dead-point support effect at each keyframe of the stance phase: 1. the equivalent QIPJCS model of single limb support; 2. the equivalent triangular truss mechanism formed by one forelimb and one hindlimb; 3. the equivalent four-link mechanism formed by one forelimb, one hindlimb, spine and ground. Then, the dynamic motion performance of the equivalent mechanism in the stance phase is analyzed: the equation between the driving torque and the landing angle is established in the case of moving at the target acceleration; therefore, energy savings can be realized by optimizing the landing angle and reducing the driving torque.

The novel QIPJCS model presented in this paper is a bionic stiffness model that is more similar to the actual animal limb and possesses better stability of motion at higher speed compared with SLIP model. Hence, this model provides a better template for the design of bionic robot limbs. Furthermore, based on the motion characteristics of the animal's natural gait, the dynamic motion mechanism of the animal limb is analyzed. According to this mechanism, an optimization method for the landing angle is presented for energy conservation and can be utilized as the joint control target of robot dynamic motion.

Funding statement

This research is funded by the University Research Program Project of Anhui Province (Grant No. 2023AH051118) and the Open Project of Anhui Province Key Laboratory of Special and Heavy Load Robot (Grant No. TZJQR012-2024 and TZJQR008-2024).

Ethics statement

Informed consent was not required for this study because this study did not involve any human samples.

Data availability statement

The datasets supporting our findings are presented in the article.

CRediT authorship contribution statement

Yi Zheng: Writing – review & editing, Writing – original draft, Visualization, Validation, Supervision, Software, Resources, Project administration, Methodology, Investigation, Funding acquisition, Formal analysis, Data curation, Conceptualization. **Sixian Rao:** Writing – review & editing, Visualization. **Jiapeng Gao:** Supervision, Software.

Declaration of competing interest

The authors declared that they have no conflicts of interest to this work.

We declare that we do not have any commercial or associative interest that represents a conflict of interest in connection with the work submitted.

Acknowledgements

We gratefully acknowledge the support of Anhui Province Key Laboratory of Special and Heavy Load Robot.

References

[1] R.L. Marsh, D.J. Ellerby, J.A. Carr, H.T. Henry, C.I. Buchanan, Partitioning the energetics of walking and running: swinging the limbs is expensive, Science 303 (5654) (2004) 80–83.
[2] M. Raibert, K. Blankespoor, G. Nelson, R. Playter, Bigdog, the rough-terrain quadruped robot, IFAC Proc. Vol. 41 (2) (2008) 10822–10825.
[3] M. Hutter, C.D. Remy, M.A. Hoepflinger, R. Siegwart, Efficient and versatile locomotion with highly compliant legs, IEEE ASME Trans. Mechatron. 18 (2) (2012) 449–458.
[4] M. Hutter, C. Gehring, D. Jud, A. Lauber, C.D. Bellicoso, V. Tsounis, J. Hwangbo, K. Bodie, P. Fankhauser, M. Bloesch, R. Diethelm, Anymal-a highly mobile and dynamic quadrupedal robot, in: In2016 IEEE/RSJ International Conference on Intelligent Robots and Systems (IROS), IEEE, 2016, pp. 38–44.
[5] J. Zico Kolter, A.Y. Ng, The stanford littledog: a learning and rapid replanning approach to quadruped locomotion, Int. J. Robot Res. 30 (2) (2011) 150–174.
[6] N.C. Sharp, Timed running speed of a cheetah (Acinonyx jubatus), J. Zool. 241 (3) (1997) 493–494.
[7] R.M. Alexander, A. Vernon, The mechanics of hopping by kangaroos (Macropodidae), J. Zool. 177 (2) (1975) 265–303.
[8] C.M. Smith, Life on the rocks: a portrait of the American mountain goat, in: Bruce L. Smith (Ed.), [book review]. The Canadian Field-Naturalist 128 (4) (2014) 420, 2014.
[9] S. Seok, A. Wang, M.Y. Chuah, D. Otten, J. Lang, S. Kim, Design principles for highly efficient quadrupeds and implementation on the MIT Cheetah robot, in: In2013 IEEE International Conference on Robotics and Automation, IEEE, 2013, pp. 3307–3312.
[10] S. Seok, A. Wang, M.Y. Chuah, D.J. Hyun, J. Lee, D.M. Otten, J.H. Lang, S. Kim, Design principles for energy-efficient legged locomotion and implementation on the MIT cheetah robot, Ieee/asme transactions on mechatronics 20 (3) (2014) 1117–1129.
[11] D.J. Hyun, S. Seok, J. Lee, S. Kim, High speed trot-running: implementation of a hierarchical controller using proprioceptive impedance control on the MIT Cheetah, Int. J. Robot Res. 33 (11) (2014) 1417–1445.
[12] D.J. Hyun, J. Lee, S. Park, S. Kim, Implementation of trot-to-gallop transition and subsequent gallop on the MIT Cheetah I, Int. J. Robot Res. 35 (13) (2016) 1627–1650.
[13] P.M. Wensing, A. Wang, S. Seok, D. Otten, J. Lang, S. Kim, Proprioceptive actuator design in the mit cheetah: Impact mitigation and high-bandwidth physical interaction for dynamic legged robots, IEEE Trans. Robot. 33 (3) (2017) 509–522.
[14] A.H. Abdulwahab, A.Z.A. Mazlan, A.F. Hawary, N.H. Hadi, Quadruped robots mechanism, structural design, energy, gait, stability, and actuators: a review study, International Journal of Mechanical Engineering and Robotics Research 12 (6) (2023).
[15] P.E. Hudson, S.A. Corr, R.C. Payne-Davis, S.N. Clancy, E. Lane, A.M. Wilson, Functional anatomy of the cheetah (Acinonyx jubatus) forelimb, J. Anat. 218 (4) (2011) 375–385.
[16] D.F. Buxton, D. Peck, Density of muscle spindle profiles in the intrinsic forelimb muscles of the dog, J. Morphol. 203 (3) (1990) 345–359.
[17] R.J. Full, D.E. Koditschek, Templates and anchors: neuromechanical hypotheses of legged locomotion on land, J. Exp. Biol. 202 (23) (1999) 3325–3332.
[18] J. Rummel, A. Seyfarth, Stable running with segmented legs, Int. J. Robot Res. 27 (8) (2008) 919–934.
[19] K.D. Mombaur, R.W. Longman, H.G. Bock, J.P. Schlöder, Open-loop stable running, Robotica 23 (1) (2005) 21–33.
[20] R.M. Ghigliazza, R. Altendorfer, P. Holmes, D. Koditschek, A simply stabilized running model, SIAM Rev. 47 (3) (2005) 519–549.
[21] A. Seyfarth, M. Günther, R. Blickhan, Stable operation of an elastic three-segment leg, Biol. Cybern. 84 (5) (2001) 365–382.
[22] D.H. Chadwick, A Beast the Color of Winter: the Mountain Goat Observed, University of Nebraska Press, Lincoln, USA, 2002.
[23] G.M. Constantinescu, Guide to Regional Ruminant Anatomy Based on the Dissection of the Goat, Iowa state university press, 2001.
[24] S. Peng, X. Ding, Revealing the mechanism of high loading capacity of the horse in leg structure, Chin. Sci. Bull. 59 (2014) 2625–2637.
[25] R. Blickhan, R.J. Full, Similarity in multilegged locomotion: bouncing like a monopode, J. Comp. Physiol. 173 (1993) 509–517.
[26] C. Couppe, M. Kongsgaard, P. Aagaard, P. Hansen, J. Bojsen-Moller, M. Kjaer, S.P. Magnusson, Habitual loading results in tendon hypertrophy and increased stiffness of the human patellar tendon, J. Appl. Physiol. 105 (3) (2008) 805–810.
[27] G.A. Lichtwark, J.C. Watson, S. Mavrommatis, A.M. Wilson, Intensity of activation and timing of deactivation modulate elastic energy storage and release in a pennate muscle and account for gait-specific initiation of limb protraction in the horse, J. Exp. Biol. 212 (15) (2009) 2454–2463.
[28] C.V. Jutte, S. Kota, Design of nonlinear springs for prescribed load-displacement functions, J. Mech. Des. 130 (8) (2008).
[29] C.T. Farley, O. Gonzalez, Leg stiffness and stride frequency in human running, J. Biomech. 29 (2) (1996) 181–186.
[30] A. Seyfarth, H. Geyer, M. Günther, R. Blickhan, A movement criterion for running, J. Biomech. 35 (5) (2002) 649–655.
[31] Z. Wróblewska, P. Kowalczyk, Ł. Płociniczak, Stability of fixed points in an approximate solution of the spring-mass running model, IMA J. Appl. Math. 88 (3) (2023) 429–454.
[32] P. Kowalczyk, Ł. Płociniczak, Z. Wróblewska, Energy variations and periodic solutions in a switched inverted pendulum model of human running gaits, Phys. Nonlinear Phenom. 443 (2023) 133554.
[33] H. Yu, M. Li, H. Cai, Analysis on the performance of the SLIP runner with nonlinear spring leg, Chin. J. Mech. Eng. 26 (5) (2013) 892–899.
[34] R.M. Alexander, Why mammals gallop, Am. Zool. 28 (1) (1988) 237–245.